

# Mechanical Metamaterials with Negative Thermal Expansion Designed through Multi-Material Topology Optimization

Zhengtong Han<sup>1,2,\*</sup>, Wentao Sun<sup>1</sup>, Yingtao Zhang<sup>1</sup>, Shayuan Weng<sup>1</sup>

<sup>1</sup>College of Mechanical and Electrical Engineering, Hohai University, Changzhou, China

<sup>2</sup>College of Mechanics and Engineering Science, Hohai University, Nanjing, China

\*Corresponding author: hzt@hhu.edu.cn

**Abstract:** Mechanical metamaterials with negative thermal expansion possess the dimensional control ability under large temperature range, and accordingly are promising in engineering applications. One challenge in developing this metamaterial through topology optimization is the potential contradiction between the thermal expansion and stiffness. Here, a multi-material topology optimization design framework was first built based on the Alternative Active Phase & Objective algorithm. Subsequently, guided by this framework, a series of metamaterials comprising two and three base materials were designed. Their deformation mechanisms were then elucidated through numerical simulation. Furthermore, influences of the material varieties on the target performances were analyzed in detail. Results showed that through giving rising to the material varieties, the bounds of the negative thermal expansion restricted by the stiffness constraints can be effectively crossed. The topology-optimized metamaterials are of extreme negative thermal expansion with the advantage of also satisfying the requirements of the elastic stiffness. The design method and resultant mechanical metamaterials are expected to provide a guideline for the engineering applications of this kind of mechanical metamaterials.

**Keywords:** Mechanical Metamaterial; Topology Optimization; Thermal Expansion; Stiffness Constraint

## 1. Introduction

The coefficient of thermal expansion (CTE) is an important thermal parameter which measures the dimensional variation of materials suffering a temperature stimulate. For myriad devices which serve under the high-temperature or in high-precision, negative thermal expansion (NTE) is urgently needed since the thermal deformations can be well purposely modulated [1]. For instance, the large temperature variations in aerospace systems pose a critical challenge, as the resulting mismatched deformations between components are a primary cause of structural failure [2]; Microelectromechanical systems [3] generally suffer the high temperature variation generated by the inner functional components, and correspondingly, the thermal deformations can cause unexpected separation and alignment errors, leading to a low spectral accuracy of the optical or functional systems.

Only a few of natural materials, e.g., special types of ceramic, oxides, and alloys [4], have negative or low CTEs due to the specific mechanisms. The magnitudes of the CTEs of these materials are generally constant and are limited within a narrow range, making it difficult to be widely used in engineering application. Mechanical metamaterials, built from artificial "meta-atoms" with tailored architectures, offer a promising alternative for achieving negative thermal expansion [5]. Typical designs include the bend-dominated [5, 6-8] and stretch-dominated [3] types.

Moreover, multi-material topology optimization [9] can be used to design such kind of mechanical metamaterials efficiently and systematically by pairing two base materials having different positive ctes according to the mathematical programming. Following the pioneering work of O. Sigmund et al. [10] on designing negative CTE metamaterials with the bi-material SIMP method, this approach has been extended to more complex scenarios involving anisotropy [11] and material uncertainty [12].

The design of load-bearing metamaterials requires a balance between thermal expansion and other mechanical properties, such as stiffness [13]. Especially, the inherent contradiction between these properties makes it difficult to achieve the metamaterials with extremal performance, as generally the arising stiffness would decrease the bounds of the thermal expansion, and vice versa [14]. Up to date, only Seth The work of Watts and Daniel A. Tortorelli [15] highlighted a critical constraint in topology-

optimized metamaterials: achieving higher stiffness comes at the cost of reduced negative thermal expansion performance.

Existing topology-optimized designs are typically limited to two materials, restricting the design space. Although work by Chen [16] shows that adding a third material can enhance NTE, its potential for balancing the critical stiffness-thermal expansion conflict remains a significant, unaddressed challenge. Accordingly, to address the above-mentioned problems, a series of bi- and tri-material metamaterials with negative thermal expansion were topology-optimized under the stiffness constraints.

This paper is structured as follows: Section 2 presents the multi-material topology optimization design framework. Section 3 analyzes the designed metamaterials, including their deformation mechanisms and the influence of material variety on thermal expansion and stiffness. Conclusions are provided in Section 4.

## 2. Multi-material topology optimization

Recently, an Alternating Active Phase & Objective (AAPO) multi-material topology optimization algorithm was proposed in our previous work [17]. The design of load-bearing metamaterials must balance stiffness with thermal expansion. This work therefore sets the explicit goal of achieving negative thermal expansion while satisfying stiffness requirements.

### 2.1 Multi-material interpolation and effective properties

For a design domain  $\Omega$  discretized by finite elements and consisted of  $M$  kinds of base materials, the design variables are the relative density of the  $m$ th base material at  $e$ th element  $\rho_{em}$ . Let these design variables be combined into a vector,  $\mathbf{p}$ . The local material properties are then calculated through the multi-material interpolation by penalizing the intermediate densities. The Young's modulus and coefficient of thermal expansion of each element  $e$  is given as:

$$\begin{cases} E_e(\mathbf{p}) = \sum_{m=1}^M \rho_{em}^p \cdot E_m^0 \\ \alpha_e(\mathbf{p}) = \sum_{m=1}^M \rho_{em}^p \cdot \alpha_m^0 \end{cases}, \quad (1)$$

Where  $E_m^0$  and  $\alpha_m^0$  are the elastic modulus and coefficient of thermal expansion (CTE) for the base material  $m$ , respectively. The term “ $p$ ” is introduced to eliminate the intermediate design variables and consequently the structures obtained are structures with clear solid-void interfaces. The value of  $p$  was set as 3.5 according to the work of O. Sigmund et al.

Then, the effective properties of the metamaterials is predicated through the asymptotic homogenization method basing on the base materials properties. The effective elastic tensor  $C^H$  and thermal stress tensor  $\beta^H$  are calculated as follows:

$$C_{ijkl}^H = \frac{1}{|Y|} \int_Y \left[ \varepsilon_{pq}^{0(ij)} - \varepsilon_{pq}^*(\chi^{ij}) \right] \cdot E_e(\mathbf{p}) \cdot \left[ \varepsilon_{rs}^{0(kl)} - \varepsilon_{rs}^*(\chi^{kl}) \right] dY, \quad (2)$$

$$\beta_{pq}^H = \frac{1}{|Y|} \int_Y \left[ \tau_{pq} - \varepsilon_{pq}^*(\psi) \right] \cdot E_e(\mathbf{p}) \cdot \left[ \varepsilon_{kl}^{0(ij)} - \varepsilon_{kl}^*(\chi^{kl}) \right] dY, \quad (3)$$

Where  $|Y|$  is the volume of the unit cell.  $\varepsilon_{pq}^{0(ij)}$  are the applied macroscopic unit fields in a planar problem.  $\tau_{pq}$  is the applied thermal load.  $\varepsilon_{rs}^*(\chi^{kl})$  and  $\varepsilon_{pq}^*(\psi)$  represent the locally varying strain field with the loading case  $kl$  and thermal load, respectively. Thus, the effective thermal expansion tensor  $\alpha^H$  can be calculated as:

$$\alpha_{ij}^H = \left( C_{ijpq}^H \right)^{-1} \cdot \beta_{pq}^H. \quad (4)$$

The periodic boundary conditions were implemented through the constraint equations method. The strain fields  $\varepsilon_{pq}^*(\chi^{ij})$  in Eq. (2) are obtained by solving the base equilibrium problem under unit test

field  $\varepsilon^0$ . As illustrated in Figure 1, the displacement on a pair of opposite boundaries consists of a macroscopic displacement field and a periodic fluctuation field  $u_i^*$ . The periodic term  $u_i^*$  is eliminated by taking the difference between the displacements on corresponding boundaries:

$$u_i^{k+} - u_i^{k-} = \varepsilon^0 (y_j^{k+} - y_j^{k-}) = \varepsilon^0 \cdot \Delta y_j^k, \quad (5)$$

Where superscripts “k+” and “k-” represents the pair of two opposite parallel boundary surfaces that are oriented perpendicular to the  $k$ -th direction. For any given parallelepiped base cell model,  $\Delta y_j^k$  is constant. Thus, with a specified  $\varepsilon^0$ , the right-hand side in Eq. (5) becomes a constant.

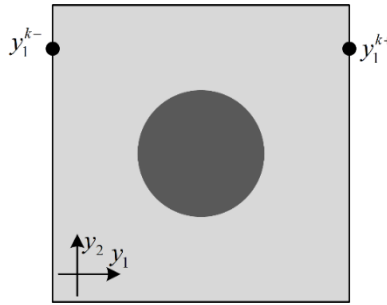


Figure 1 Illustration of the node set categorization for a two-dimensional model.

## 2.2 Topology optimization framework

The AAPO algorithm converts the original problem into binary-phase sub-problems, where the material properties for each element are calculated from the two active phases 'a' and 'b' using Eq. (1):

$$\begin{cases} E_e(\boldsymbol{\rho}) = \rho_{ea}^p \cdot E_a^0 + (r_e - \rho_{ea})^p \cdot E_b^0 + \sum_{m=1, m \neq a, b}^M \rho_{em}^p \cdot E_m^0 \\ \alpha_e(\boldsymbol{\rho}) = \rho_{ea}^p \cdot \alpha_a^0 + (r_e - \rho_{ea})^p \cdot \alpha_b^0 + \sum_{m=1, m \neq a, b}^M \rho_{em}^p \cdot \alpha_m^0 \end{cases}, \quad (6)$$

Where

$$r_e = 1 - \sum_{m=1, m \neq a, b}^M \rho_{em}. \quad (7)$$

In cases where all active phases in an AAPO subproblem are solid, the objective function aims for a negative CTE:

$$\text{minimize: } ft = \sum_{i,j}^d w_{ij} \cdot \alpha_{ij}^H, \quad (8)$$

Where  $w_{ij}$  are the adjusting factors associated with the corresponding thermal strain tensor. For a two-dimensional problem, the  $C^H$  represents the effective elasticity tensor which can be written as follow:

$$C^H = \begin{bmatrix} C_{11} & C_{12} & C_{13} \\ & C_{22} & C_{23} \\ \text{Syms} & & C_{33} \end{bmatrix}. \quad (9)$$

Then, the bulk modulus is chosen as the stiffness constraints, which is defined as:

$$fs(\boldsymbol{\rho}) = C_{11} + C_{22} + C_{12} + C_{21} - S^* \geq 0, \quad (10)$$

Where the  $S^*$  represents the predefined lower bound of the stiffness constraints. Incorporating the volume constraints, we establish the optimization subproblem as:

$$\begin{aligned} &\text{Find : } \rho_{ea} (e \in \mathbf{Ne}) \\ &\min : f(\mathbf{p}) = ft \\ &\text{s.t.:} \begin{cases} fs(\mathbf{p}) = C_{11} + C_{22} + C_{12} + C_{21} - S^* \geq 0 \\ fv(\mathbf{p}) = \sum_{e \in \mathbf{Ne}} \rho_{ea}(\mathbf{x}) v_e - V_a^* \leq 0 \\ 0 \leq \rho_{ea} \leq 1, e \in \mathbf{Ne} \end{cases} \end{aligned} \quad (11)$$

In the case where one of the active phases is void, the optimization objective becomes the maximization of the bulk modulus subject to the volume constraints, formulated as:

$$\begin{aligned} &\text{Find : } \rho_{ea} (e \in \mathbf{Ne}) \\ &\min : f(\mathbf{p}) = -fs(\mathbf{p}) \\ &\text{s.t.:} \begin{cases} fv(\mathbf{p}) = \sum_{e \in \mathbf{Ne}} \rho_{ea}(\mathbf{x}) v_e - V_a^* \leq 0 \\ 0 \leq \rho_{ea} \leq 1, e \in \mathbf{Ne} \end{cases} \end{aligned} \quad (12)$$

The workflow of the proposed design framework is illustrated in Figure 2. The algorithm begins by selecting two active phases, denoted as 'a' and 'b'. A SIMP-based subproblem is then constructed. The objective function and the maximum inner-loop iterations (IterIn\_max) for this subproblem are determined by the nature of the active phases. If one phase is void, Eq. (12) is used to maximize stiffness, as the CTE cannot be optimized, and IterIn\_max is set to IterInP. Conversely, if both phases are solid, Eq. (11) is applied to minimize the CTE, with IterIn\_max set to IterInT. This process repeats until the maximum number of outer-loop iterations (IterOut\_max) is reached.

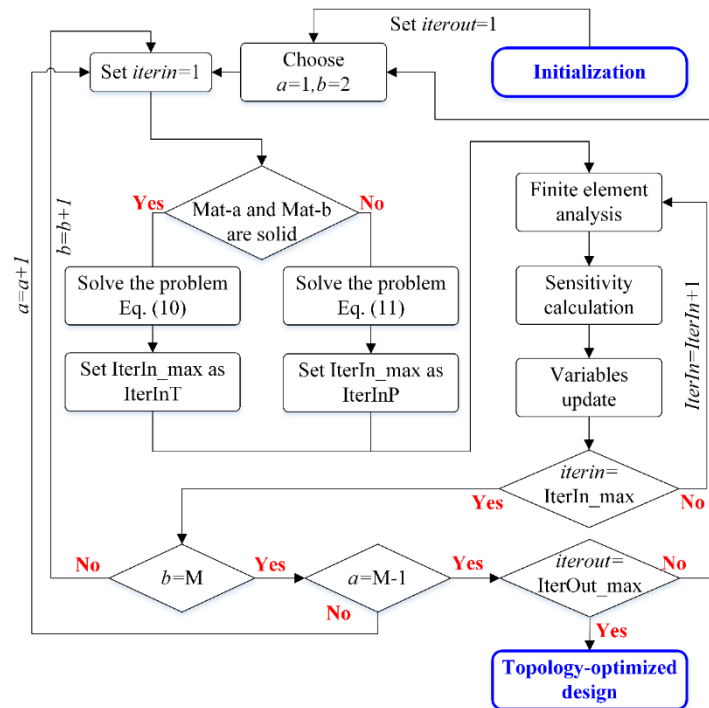


Figure 2 Flow chart for designing mechanical metamaterials with negative thermal expansion under the stiffness constraints.

### 3. Results and discussion

To analyze the influence of base material category on the topological design, two numerical examples were investigated. For each, metamaterials with negative thermal expansion were designed under stiffness constraints of 0.5%, 10%, and 15% of the maximum base material Young's modulus. Table 1 lists all relevant material properties and volume constraints. Note that the Mat-1 and Mat-3 defined in the Example 2 were the same as the Mat-1 and Mat-2 defined in the Example 1, while a new base material Mat-2 with moderate property was introduced. These dimensionless values were chosen according to

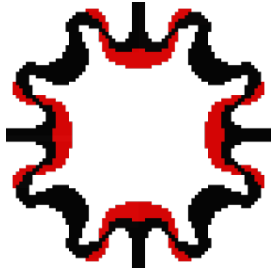
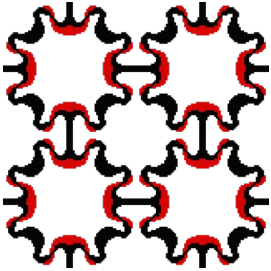
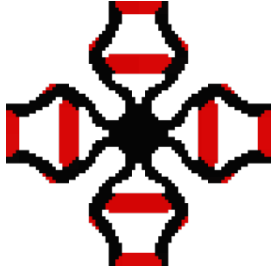
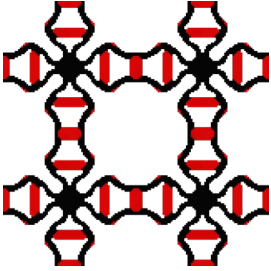
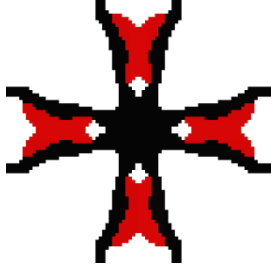
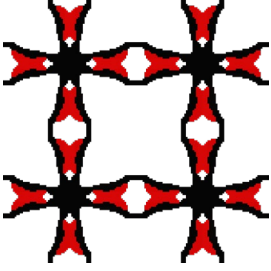
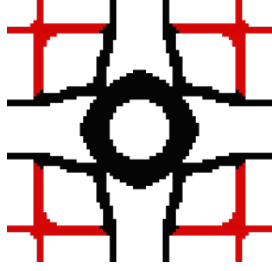
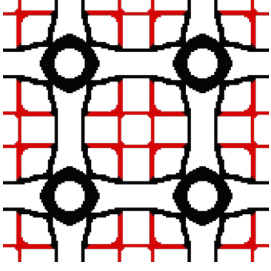
typical examples presented in Ref. The design domain of all the examples was set as a two-dimensional dimensionless square ( $80 \times 80 \text{ mm}^2$ ) with periodic boundary conditions and octant symmetric constraints. Other parameters kept consistent in all the examples.

*Table 1 Materials and corresponding properties used in the numerical examples.*

Example	Material	Young's modulus (MPa)	Coefficient of thermal Expansion (ppm/°C)	Poisson's ratio	Volume constraint	Colour
1	Mat-1	10	1	0.3	0.3	Black
	Mat-2	1	10	0.3	0.1	Red
2	Mat-1	10	1	0.3	0.2	Black
	Mat-2	5	2	0.3	0.1	Blue
	Mat-3	1	10	0.3	0.1	Red

### 3.1 Bi-material metamaterials under stiffness constraints

*Table 2 Topology optimization results of the bi-material mechanical metamaterials. (The effective properties are of dimensionless values)*

Stiffness constraints	Unit cell	Metamaterials	Effective properties
None			Effective elastic tensor = $\begin{bmatrix} 0.0168 & 0.0097 & 0 \\ 0.0097 & 0.0168 & 0 \\ 0 & 0 & 0.0077 \end{bmatrix}$ Bulk modulus = 0.053 CTE = -3.158
5%			Effective elastic tensor = $\begin{bmatrix} 0.3336 & 0.0074 & 0 \\ 0.0074 & 0.3336 & 0 \\ 0 & 0 & 0.0037 \end{bmatrix}$ Bulk modulus = 0.682 CTE = -0.752
10%			Effective elastic tensor = $\begin{bmatrix} 0.5639 & 0.0726 & 0 \\ 0.0726 & 0.5639 & 0 \\ 0 & 0 & 0.0134 \end{bmatrix}$ Bulk modulus = 1.273 CTE = -0.248
15%			Effective elastic tensor = $\begin{bmatrix} 0.9973 & -0.1353 & 0 \\ -0.1353 & 0.9973 & 0 \\ 0 & 0 & 0.0097 \end{bmatrix}$ Bulk modulus = 1.724 CTE = 0.181

The topology optimization results for two-material metamaterials are summarized in Table 2, presenting the unit cell configuration, periodic array, and effective properties. The domains of Mat-1 and Mat-2 are colored black and red in the following figures. In view of the outline of the topological configuration, design results under various stiffness constrains are quite different. Without stiffness

constraint, the magnitude of the CTE of the metamaterial in the first column of Table 2 (-3.158) is much higher than that of the others (-0.752, -0.248). As shown in the contours on the deformed shape (Fig.3 (a)) obtained through the finite element analysis (FEA), the thermal strains  $\varepsilon_T$  under the temperature variations  $\Delta T = 0.01^\circ\text{C}$  is of -3.21%. Accordingly, the numerically calculated CTE is -3.21, which is quite close to the topology-optimized results.

To elucidate the deformation mechanism, a representative unit cell is extracted in Figure 3(b). As highlighted, regions of Mat-2 (red, high CTE) are distributed along the edges of Mat-1 (black, low CTE), forming a characteristic bi-material rib layout. Upon heating, the large expansion of the Mat-2 ribs forces the adjacent Mat-1 ribs to bend inward, resulting in macroscopic shrinkage — i.e., negative thermal expansion — in both horizontal and vertical directions.

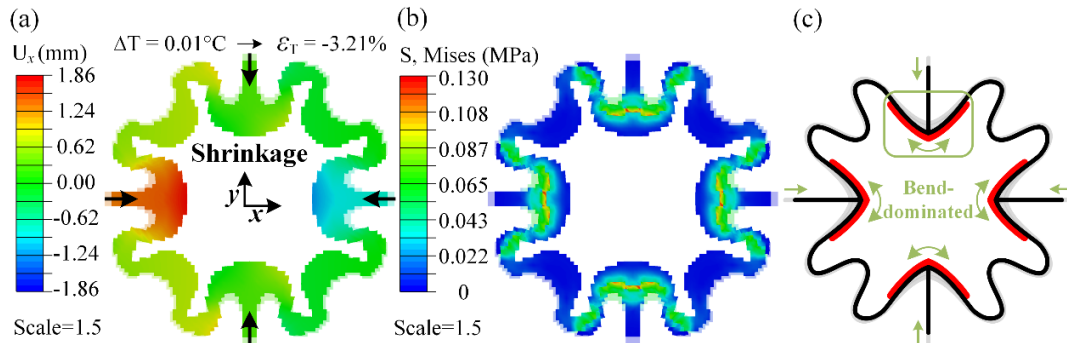


Figure 3 Numerical simulations results of the bi-material design without stiffness constraints: (a) Contour of displacement field; (b) Contour of von Mises stress field; (c) Illustration of deformation mechanism.

Increasing stiffness constraints transform the bi-material layout from a rib-based to a hinged structure (Figure 4b), shifting the deformation mechanism from bending- to stretch-dominated. The net thermal expansion arises from the competition between rib shrinkage and enlargement. Under the highest constraint (15%), the appearance of positive thermal expansion (Table 2, fourth column) signifies the limit of the bi-material design strategy.

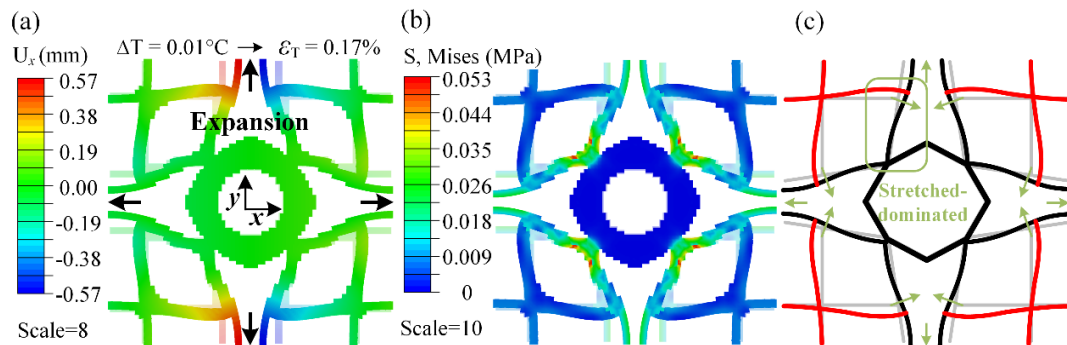


Figure 4 Numerical simulations results of the bi-material design under the stiffness constraint of 15% Young's modulus of the base material Mat-1: (a) Contour of displacement field; (b) Contour of von Mises stress field; (c) Illustration of deformation mechanism.

### 3.2 Tri-material metamaterials under stiffness constraints

The results (Table 3) show that while the material layouts differ significantly from bi-material designs, their overall geometries are similar. A comparison under the 15% stiffness constraint reveals that the key high-CTE (Mat-3, red) crossed ribs, essential for deformation, are almost identical.

However, as marked by the rectangle in Figure 5(b), parts of the Mat-1 (black, low CTE and high Young's modulus) in the tri-material design were replaced by the Mat-2 (blue, middle CTE and middle Young's modulus) in the tri-material design. The local stiffness of the tri-material design is therefore weakened, resulting in a larger shrinkage deformation at the boundary. The CTE of the tri-material design is exactly negative, which is consistent with the objective. It's obvious that the variety in base materials could effectively improve the magnitudes of the CTE, while has a negligible influence on the

deformation pattern.

Table 3 Topology optimization results of the tri-material mechanical metamaterials. (The effective properties are of dimensionless values)

Stiffness constraints	Unit cell	Metamaterials	Effective properties
None			Effective elastic tensor = $\begin{bmatrix} 0.0086 & 0.0049 & 0 \\ 0.0049 & 0.0086 & 0 \\ 0 & 0 & 0.0036 \end{bmatrix}$ Bulk modulus = 0.027 CTE = -4.208
5%			Effective elastic tensor = $\begin{bmatrix} 0.2681 & 0.0029 & 0 \\ 0.0029 & 0.2681 & 0 \\ 0 & 0 & 0.0040 \end{bmatrix}$ Bulk modulus = 0.542 CTE = -0.914
10%			Effective elastic tensor = $\begin{bmatrix} 0.4542 & 0.0948 & 0 \\ 0.0948 & 0.4542 & 0 \\ 0 & 0 & 0.0081 \end{bmatrix}$ Bulk modulus = 1.098 CTE = -0.387
15%			Effective elastic tensor = $\begin{bmatrix} 0.8709 & -0.0839 & 0 \\ -0.0839 & 0.8709 & 0 \\ 0 & 0 & 0.0120 \end{bmatrix}$ Bulk modulus = 1.574 CTE = -0.107

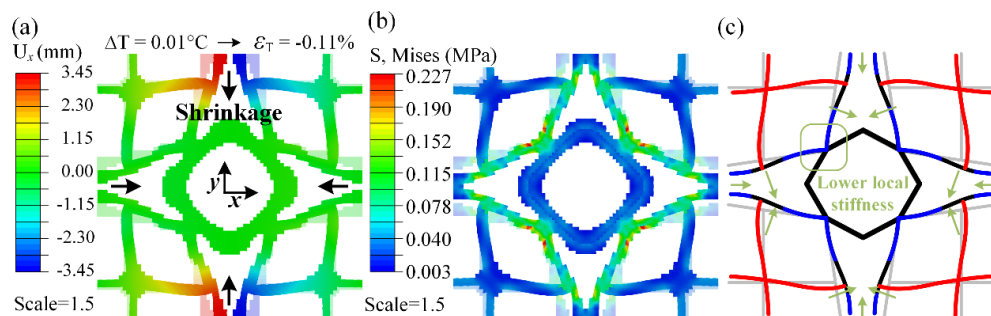


Figure 5 Numerical simulations results of the tri-material design under the stiffness constraint of 15% Young's modulus of the base material Mat-1: (a) Contour of displacement field; (b) Contour of von Mises stress field; (c) Illustration of deformation mechanism.

### 3.3 Influences of material varieties

To clarify the impact of material variety on the designs, the results are replotted in Figure 6, with effective stiffness on the horizontal axis and CTE magnitude on the vertical axis. For bi-material



metamaterials, the CTE reaches its maximum value without stiffness constraints but decreases sharply by 92.14% as the stiffness requirement increases. Notably, under a high stiffness constraint of 1.5 MPa, the CTE becomes positive, diverging completely from the design objective. Tri-material designs show a consistent trend, with the CTE dropping by 94.99%. These results demonstrate that excessively high stiffness constraints severely inhibit the achievement of extreme negative thermal expansion.

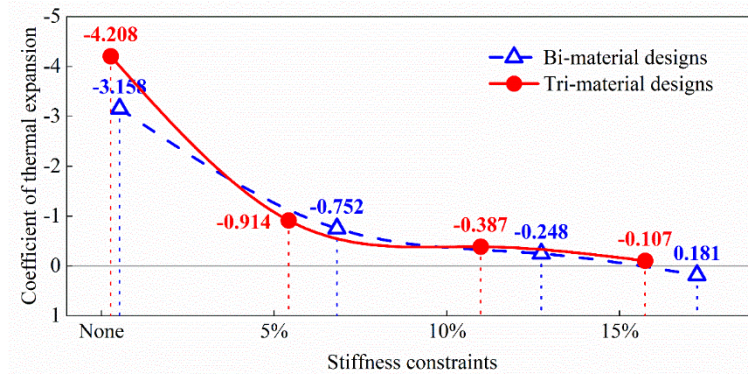


Figure 6 Comparison between the topology-optimized bi- and tri-material metamaterials under different stiffness constraints.

Another tendency revealed in Figure 6 is that the magnitudes of the CTEs of the tri-material designs are generally higher those of the bi-material designs. Especially, when the stiffness constraint is largely increased to 1.5 MPa, the tri-material design presents an exactly negative thermal expansion performance, while the bi-material design is of positive CTE. In combination with the abscissa, it's obvious that the actual bulk modulus of the designs is generally higher than the pre-defined stiffness constraints. In the optimization problem, the objective function has higher priority over the constraint function. Herein, the topology optimization problems were formulated for designing metamaterials with negative thermal expansion under stiffness constraints, which is responsible for the difference between the predefined stiffness constraints and actual effective stiffness. As clearly illustrated in Figure 6, the resultant gaps in the tri-material design are significantly lower than that in the bi-material designs. Combing with the revealed deformation mechanisms in Figure 4(b) and Figure 5(b), the local stiffness of the metamaterials can be finely tuned with more kinds of base materials, which is responsible for the improvements of the CTEs between the tri- and bi-material designs.

#### 4. Conclusions

This study presented a topology optimization framework for designing mechanical metamaterials that balance negative thermal expansion (NTE) with stiffness constraints. We successfully designed eight bi- and tri-material metamaterials, quantitatively demonstrating that tri-material designs generally achieve higher NTE magnitudes. This indicates that increasing material variety can alleviate the inherent conflict between NTE and stiffness, as more materials allow finer tuning of local stiffness to enhance deformation mechanisms. Our work provides a valuable guideline for designing functional metamaterials satisfying multi-physical requirements. Future work should explore designs with real materials and advance the manufacturing of complex multi-material architectures.

#### Acknowledgements

This research was funded by the China Postdoctoral Science Foundation (Grant No. 42408902), and Natural Science Research of Jiangsu Higher Education Institutions of China (Grant No. 524047011), The Central University Startup Fund (Grant No. B250201080), and the National Natural Science Foundation of China Youth Fund (Grant No. 12302130).

#### Declaration of Competing Interest

The authors declare that they have no known competing financial interests or personal relationships.



## References

- [1] Wei K, Peng Y, Qu Z, Pei Y, Fang D. A cellular metastructure incorporating coupled negative thermal expansion and negative Poisson's ratio. *Int. J. Solids Struct.* 2018;150:255-267.
- [2] Dong K, Peng X, Zhang J, Gu B, Sun B. Temperature-dependent thermal expansion behaviors of carbon fiber/epoxy plain woven composites: Experimental and numerical studies. *Compos. Struct.* 2017; 176: 329-341.
- [3] Wang P, Liu Y, Wang D, Liu H, Liu W, Xie H. Stability study of an electrothermally-actuated MEMS mirror with Al/SiO<sub>2</sub> bimorphs. *Micromachines.* 2019;10:693.
- [4] Miller W, Smith C, Mackenzie D, Evans K. Negative thermal expansion: a review. *J. Mater. Sci.* 2009;44:5441-5451.
- [5] Dong HW, Zhao SD, Wei P, Cheng L, Wang YS, Zhang C. Systematic design and realization of double-negative acoustic metamaterials by topology optimization. *Acta Mater.* 2019;172:102-120.
- [6] Lim TC. 2D metamaterial with in-plane positive and negative thermal expansion and thermal shearing based on interconnected alternating bimaterials. *Mater. Res. Express.* 2019; 6(11): 115804.
- [7] Luo W, Xue S, Zhang M, Zhao C, Li G. Bi-material negative thermal expansion inverted trapezoid lattice based on a composite rod. *Materials.* 2019;12:3379.
- [8] Parsons EM. Lightweight cellular metal composites with zero and tunable thermal expansion enabled by ultrasonic additive manufacturing: Modeling, manufacturing, and testing. *Compos. Struct.* 2019; 223: 110656.
- [9] Sigmund O, Maute K. Topology optimization approaches. *Struct. Multidiscip. Optim.* 2013;48:1031-1055.
- [10] Sigmund O, Torquato S. Composites with extremal thermal expansion coefficients. *Applied Physics Letters.* 1996;69:3203-3205.
- [11] Takezawa A, Kobashi M. Design methodology for porous composites with tunable thermal expansion produced by multi-material topology optimization and additive manufacturing. *Composites Part B: Engineering.* 2017;131:21-29.
- [12] Li H, Li H, Xiao M, Zhang Y, Fu J, Gao L. Robust topology optimization of thermoelastic metamaterials considering hybrid uncertainties of material property. *Compos. Struct.* 2020;248:112477.
- [13] Chen J, Xu W, Wei Z, Wei K, Yang X. Stiffness characteristics for a series of lightweight mechanical metamaterials with programmable thermal expansion. *I. J. Mech. Sci.* 2021;202:106527.
- [14] Gibiansky L, Torquato S. Thermal expansion of isotropic multiphase composites and polycrystals. *J. Mech. Phys. Solids* 1997;45:1223-1252.
- [15] Watts S, Tortorelli DA. Optimality of thermal expansion bounds in three dimensions. *Extreme Mech. Lett.* 2017;12:97-100.
- [16] Chen MM, Fu MH, Lin-Hua, Sheshenin SV. A novel 3D structure with tunable Poisson's ratio and tailorable coefficient of thermal expansion based on a tri-material triangle unit. *Compos. Struct.* 2020: 112803.
- [17] Han Z, Wei K. Multi-material topology optimization and additive manufacturing for metamaterials incorporating double negative indexes of Poisson's ratio and thermal expansion. *Addit. Manuf.* 2022; 54: 102742.